

Calibration of Cone Penetration Test in Sand

HUAI-HOUH HSU AND AN-BIN HUANG

Department of Civil Engineering
National Chiao-Tung University
Hsinchu, Taiwan, R.O.C.

(Received October 1, 1998; Accepted April 21, 1999)

ABSTRACT

Due to its simplicity, the cone penetration test (CPT) is a popular in-situ testing method. CPT is especially desirable in characterizing sand where it is difficult to obtain undisturbed samples. Because of the large strain which occurs during a cone penetration, theoretical analysis of CPT results has been difficult and, hence, limited. Accordingly, interpretation of CPT data is mostly based on empirical correlations. Some of the empirical correlations are based on CPT in the calibration chambers. An important drawback of interpreting CPT in a calibration chamber is its boundary effects. Correction factors have been proposed to account for these boundary effects. However, the validity of the use of correction factors and the mechanisms of boundary effects have not been independently verified. The authors have developed an axisymmetric field simulator in which CPT calibration tests can be conducted under substantially reduced boundary effects. A series of CPT calibration tests has been performed in the new simulator system to correlate the cone tip resistance (q_c) with the stress state. Results show that the correlation of q_c and the initial effective mean normal stress (prior to cone penetration) is clearer than the other components of the initial stress state. However, under the same initial effective mean normal stress, q_c has a consistent localized relationship with the initial horizontal stress. q_c is affected by the horizontal stress near the cone tip, where there exists an obvious correlation between them. This paper introduces chamber calibration tests of CPT, describes this new field simulator system, presents available CPT data obtained using the new simulator and discusses the stress state affected q_c values.

Key Words: cone penetration test, sand, dilatancy, stress state, calibration chamber test

1. Introduction

Because of the lack of cohesion, it is essentially impossible to obtain undisturbed samples in sand. The Cone Penetration Test (CPT) is an efficient tool used to determine the engineering properties of sand, in situ. Results of CPT in sand typically include the cone tip resistance (q_c), sleeve friction (f_s) and friction ratio ($F_R=f_s/q_c$). The main purpose of CPT in sand usually is to determine the in situ state of stress, relative density (D_r) or void ratio (e), and friction angle (ϕ'). The combination of q_c and F_R can be used in soil classification (e.g., Robertson *et al.*, 1986), and available methods generally agree with one another. However, such agreement is less obvious when the interpretation of CPT goes beyond soil classification.

Over the past few decades, many theories and experimental procedures have been proposed to interpret q_c values. These theories basically treat cone penetration either as a bearing capacity failure (e.g., Janbu and Senneset, 1974; Durgunoglu and Mitchell, 1975) or a cavity expansion (e.g., Vesic, 1972; Baligh, 1976; Yu and Houlsby, 1991; Salgado, 1993; Salgado

et al., 1997). In the first case, q_c is related to the strength and stress parameters through a limiting equilibrium under an assumed bearing capacity failure mechanism. In the second case, q_c is related to the cavity expansion limiting pressure (P_1), which in turn is a function of the soil strength and stress parameters. CPT is a large strain problem, and the success of these theoretical analyses has been limited.

The laboratory chamber calibration test offers an experimental or empirical way to interpret results of CPT. Uniform sand specimens can be prepared in the chamber with known stress conditions and density. Results of CPT obtained in the chamber can then be compiled to derive empirical interpretation procedures. A typical method that uses q_c to infer D_r or the shear strength parameter (i.e., ϕ') normally involves the state of stress. The initial (prior to cone penetration) horizontal stress (σ'_{ho}) (Houlsby and Hitchman, 1988), vertical stress (σ'_{vo}), and mean normal stress (σ'_{oo}) (e.g., Schmertmann, 1976; Villet and Mitchell, 1981; Jamiolkowski *et al.*, 1988) have all been proposed for coupling with either D_r or ϕ' as part of the interpretation for q_c . No consensus has been reached, however, as

to which one of the above postulations is more acceptable. The main obstacle in reaching a conclusion is that the conventional calibration chamber imposes significant boundary effects on CPT. Theories and empirical methods (Baldi *et al.*, 1982; Mayne and Kulhawy, 1991; Salgado, 1993) have been proposed to correct for the boundary effects. These correction factors again have different views on the relationship between q_c and state of stress. There is little physical evidence where CPT is performed in a controlled environment with known initial stress conditions and no (or insignificant) boundary effects to validate any of the above statements regarding the relationships among q_c , D_r (or ϕ') and the state of stress.

As part of a research project funded by the National Science Council of the R.O.C., the authors have developed a calibration chamber system in which CPT can be performed under simulated field conditions. A series of CPT calibration tests have been performed in clean, uniformly graded quartz sand using the new simulator system. The q_c values obtained in the simulator have been compared with some of the existing postulations or interpretation methods. This paper introduces the basic concept of CPT calibration tests, describes this new field simulator system and presents available CPT data obtained under simulated field conditions.

II. Chamber Calibration Tests of CPT in Sand

The idea of calibrating CPT in sand is believed to have been developed by Holden (1991) at the Country Roads Board (CRB), Melbourne, Victoria, Australia, in the late 1960's. The calibration chamber as shown in Fig. 1 consists of a large cylindrical specimen of sand, enclosed in a rubber membrane and loaded laterally by a water jacket. The chamber itself is somewhat similar to a large triaxial cell. A cavity-wall or

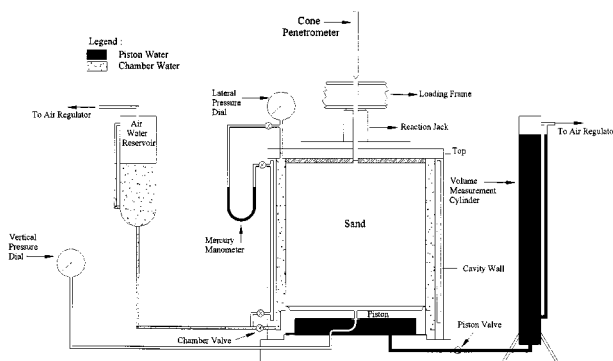


Fig. 1. Setup of a conventional calibration chamber.

Table 1. Boundary Conditions in Conventional Calibration Chamber Tests

Boundary conditions	Top & bottom boundary		Lateral boundary	
	Stress	Strain	Stress	Strain
B1	Constant	–	Constant	–
B2	–	0	–	0
B3	Constant	–	–	0
B4	–	0	Constant	–

double-wall is used to assure rigidity in the lateral direction when zero lateral strain (K_0) conditions are imposed on the specimen. By maintaining a cavity pressure that is equal to the chamber pressure, full rigidity of the inner-wall is effectively established.

A typical cavity-wall calibration chamber is capable of creating four types of boundary conditions as shown in Table 1. Been *et al.* (1988) indicated that boundary conditions on the top and bottom of the chamber specimen have little effect on CPT test results. Parkin (1988) stated that of the four boundary conditions, the most significant are B1 and B3. Houlsby and Hitchman (1988) stated that q_c has no consistent correlation when σ'_{vo} is applied in the chamber under B1 conditions.

The calibration chamber has been an important research tool for use in establishing interpretation procedures for CPT in sand. According to statistics obtained by Ghionna and Jamiolkowski (1991), there were 19 calibration chambers in the world in 1991. More calibration chambers have been built (e.g., Peterson and Arulmoli, 1991; Hsu and Huang, 1998) since then. The applications of calibration chambers have also been extended to other types of in situ testing methods. These applications have included the Marchetti dilatometer (Borden, 1991), pressuremeter (Huang *et al.*, 1991), hydraulic fracture (Been and Kosar, 1991) and calibration of pile foundations (Kulhawy, 1991; O'Neill, 1991). Table 2 shows a summary of the currently available calibration chambers in the world. The National Chiao-Tung University (NCTU) operates two calibration chamber systems. One of them is a medium sized conventional calibration chamber originally built at Clarkson University in the U.S. The other is the newly developed field simulator, which will be described in detail later in this paper.

Some of the most significant advantages of conducting CPT in a calibration chamber include: (1) repeatability of the test and use of the specimen, (2) uniformity of the specimen, and (3) controlled and known boundary conditions and stress history. These advantages, plus the fact that it is essentially impossible to obtain undisturbed samples in sand, make cali-

Calibration of Cone Penetration Test in Sand

Table 2. Current Calibration Chambers in the World

Calibration chamber (Owner and location)	Specimen diameter	Specimen height	Boundary conditions		
			Radial	Bottom	Top
		m			
Country Roads Board, Australia	0.76	0.91	Flexible	Cushion	Rigid
University of Florida, U.S.A.	1.20	1.20	Flexible	Cushion	Rigid
Monash University, Australia	1.20	1.80	Flexible	Cushion	Rigid
Norwegian Geotechnical Institute	1.20	1.50	Flexible	Cushion	Rigid
ENEL-CRIS, Milano, Italy	1.20	1.50	Flexible	Cushion	Rigid
ISMES, Bergamo, Italy	1.20	1.50	Flexible	Cushion	Rigid
University of California, Berkeley, U.S.A.	0.76	0.80	Flexible	Rigid	Rigid
University of Texas at Austin, U.S.A.	Cube 2.1×2.1×2.1		Flexible	Flexible	Flexible
University of Houston, U.S.A.	0.76	2.54	Flexible	Cushion	Cushion
North Carolina State University, U.S.A.	0.94	1.00	Flexible	Rigid	Rigid
Louisiana State University, U.S.A.	0.55	0.80	Flexible	Flexible	Rigid
Golder Associates, Calgary, Canada	1.40	1.00	Flexible	Rigid	Cushion
Virginia Polytechnic Institute and State University, U.S.A.	1.50	1.50	Flexible	Rigid	Rigid
University of Grenoble, France	1.20	1.50	Flexible	Cushion	Cushion
Oxford University, U.K.	0.90	1.10	Flexible	Cushion	Rigid
University of Tokyo, Japan	0.90	1.10	Flexible	Rigid	Rigid
University of Sheffield, U.K.	0.79	1.00	Flexible	Rigid	Flexible
Cornell University, U.S.A.	2.10	2.90	Flexible	Rigid	Rigid
Waterways Experiment Station, U.S.A.	0.80-3.00	Variable	Flexible	Rigid	Rigid
National Chiao-Tung University, Taiwan, R.O.C.	0.51	0.76	Flexible	Rigid	Rigid
National Chiao-Tung University, Taiwan, R.O.C.	0.79	1.60	Flexible	Flexible	Flexible

Source: Ghionna and Jamiolkowski (1991)

bration chamber testing a rather desirable tool in establishing correlations between CPT and engineering properties for sands and other materials.

Among other drawbacks of performing tests in freshly deposited sand is the finite dimension of the chamber specimen. A standard cone penetrometer has a diameter of 35.7 mm. The diameter ratio (R_d) of the chamber specimen (D) to that of a standard cone is approximately 42 even for a relatively large 1.5m-diameter chamber specimen. Ideally, R_d is infinite in the field. Previous studies on the use of chamber calibration tests have indicated that the field conditions for CPT where the soil extends laterally to infinity is expected to be between the B1 and B3 conditions (Veismanis, 1974; Parkin, 1988). The cone tip resistance, q_c , under B3 confinement, continues to increase with the depth and does not reach a “plateau” in dense sand (Parkin and Lunne, 1982; Parkin, 1988). Parkin and Lunne (1982) compiled CPT data under different boundary conditions; D_r and R_d are shown in Fig. 2. For loose sand, chamber results are relatively independent of boundary conditions, even when R_d is as low as 21. For dense sand, all calibration chamber results are affected by boundary conditions, even for an R_d value of 60 or greater. For tests under B1 conditions, q_c is mostly a function of σ'_{ho} , at least up to the overconsolidation ratio (OCR) of 8 (Veismanis, 1974; Chapman and Donald, 1981; Parkin, 1988;

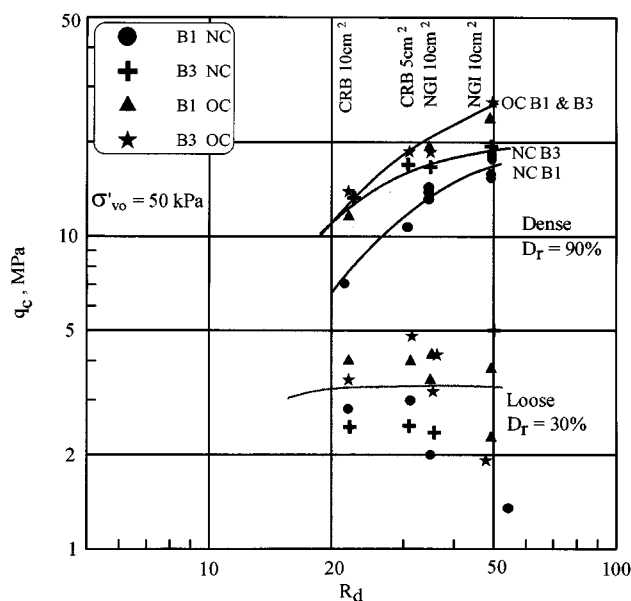


Fig. 2. q_c under different boundary conditions, D_r and R_d . [Adapted from Parkin and Lunne (1982)]

Houlsby and Hitchman, 1988).

In order to account for boundary effects, Baldi *et al.* (1982) proposed an empirical correction factor (referred to as r) which is a function of R_d , and increases with D_r and the overconsolidation ratio. However,

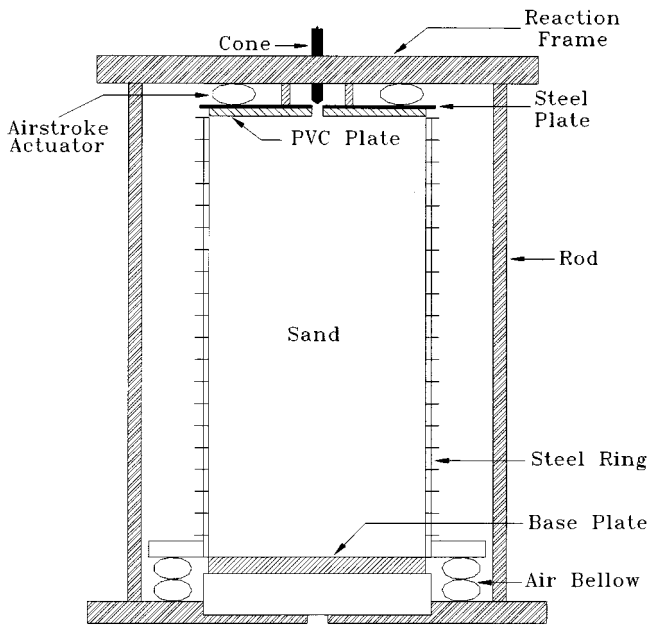


Fig. 3. Schematic diagram of the simulator.

based on analysis of their database, Mayne and Kulhaw (1991) proposed that r is related to D_r and R_d only. Salgado (1993) stated that the major influential factors are D_r , R_d , the state of initial stress and some of the intrinsic parameters of sand. The validity of these correction methods has yet to be verified independently by performing CPT in sand with known density, stress conditions and under no boundary effects.

III. Calibration of CPT under Simulated Field Conditions

Huang and Ma (1994) used the distinct element method (DEM) coupled with the boundary element method (BEM) to simulate CPT in a granular material with infinite boundary conditions. Results obtained by Huang and Ma (1994) have indicated the effectiveness of minimizing boundary effects using BEM simulations. The success and experience gained in earlier attempts inspired the authors to develop an axisymmetric field simulator in which CPT calibration tests could be conducted under substantially reduced boundary effects (Hsu and Huang, 1998).

The new simulator system at NCTU consists of a sand rainer, chamber rings, an electronic data logging and control unit, a pneumatic system, a reaction frame system, and a hydraulic system.

Figure 3 shows a schematic diagram of the fully assembled calibration chamber system. The diameter and height of the sand specimen are 790 mm and 1600 mm, respectively. The vertical boundary is stress

controlled only. The vertical stress is applied through four airstroke actuators attached to the reaction frame. The lateral boundary consists of a stack of rings. This is the main difference between the conventional chamber and the new simulator. The simulator rings are lined with an inflatable silicone rubber membrane on the inside to facilitate boundary displacement measurement and stress control. Four air bellows inflated at constant pressure are placed at the bottom of the ring stack. This system, similar to the concept of a floating ring in an oedometer, reduces frictional forces between sand and rubber membranes.

A sand rainer similar to that described by Rad and Tumay (1987) is used to prepare the specimen. The specimen is prepared by pluviation from a hopper through a perforated plate and two diffuser meshes. The uniformity and density can be well controlled by means of this arrangement and by controlling the diameter of the holes in the perforated plate. The lateral boundary is set to be rigid, simulating K_0 conditions, during sand pluviation.

The membrane expansion measuring system consists of a wax lubricated, heavy duty fishing line wrapped around the membrane. The ends of the fishing line are attached to a piece of delrin chain and then to a spring loaded extensometer. The extensometer, instrumented with full bridged strain gauges, tightens the fishing line and senses the circumferential displacement of the rubber membrane. Figure 4 shows a schematic and cross sectional view of the simulator ring and its membrane.

A field simulation consists of a physical cylindrical specimen and a numerically simulated soil mass that extends laterally from the physical boundary to infinity. Numerical simulation of the soil mass is

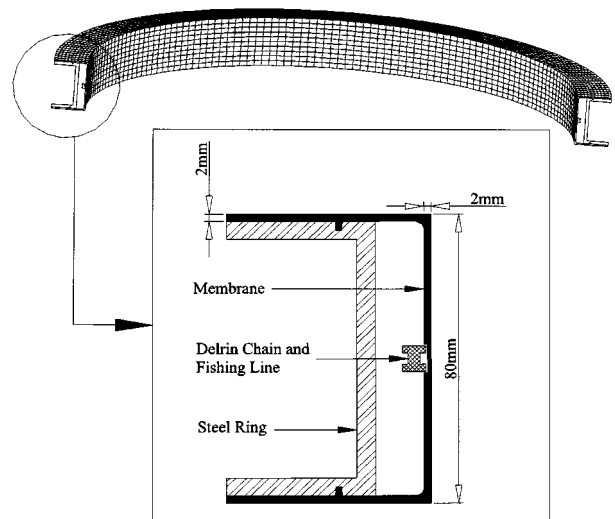


Fig. 4. Cross sectional view of a simulator ring.

Calibration of Cone Penetration Test in Sand

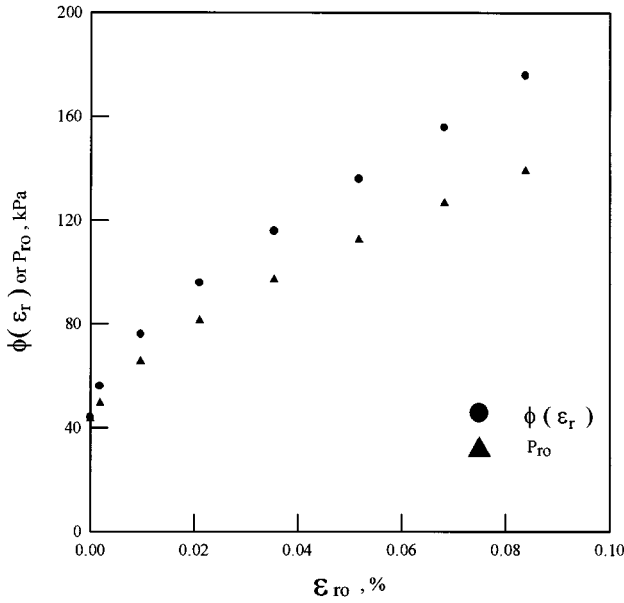


Fig. 5. $\phi(\epsilon_r)$ and the $P_{ro}-\epsilon_{ro}$ curves.

conducted based on the cylindrical cavity expansion theory. The stress-strain relationship of the sand specimen is directly measured by means of a lateral compression test on the specimen. The relationship between stress (P_{ro}) and radial strain (ϵ_{ro}) at the physical-simulated interface is then derived by means of integration from the physical boundary to infinity:

$$P_{ro} = \sigma_{ho} + \int_0^{\epsilon_{ro}} \frac{\phi(\epsilon_r)}{2\epsilon_r} d\epsilon_r, \quad (1)$$

where

$\phi(\epsilon_r)$ = the stress strain relationship measured by means of a lateral compression test on the sand specimen;

ϵ_r = the strain in the radial direction.

The derived $P_{ro}-\epsilon_{ro}$ relationship is stored in the computer. During cone penetration, the boundary displacements and stresses are measured and individually controlled at each ring level. The circumferential displacement at the boundary of each ring level, ΔC , is converted to ϵ_{ro} :

$$\epsilon_{ro} = \frac{\Delta C}{\pi D}, \quad (2)$$

where D = the diameter of the physical specimen.

P_{ro} in response to ϵ_{ro} under simulated field conditions is determined in accordance with the recorded $P_{ro}-\epsilon_{ro}$ relationship. Figure 5 shows the $\phi(\epsilon_r)$ value

obtained from the lateral compression test and the corresponding $P_{ro}-\epsilon_{ro}$ curve. During penetration, P_{ro} for each ring level is adjusted pneumatically and continuously updated with the change of ΔC .

A hydraulic piston equipped with a proportional valve, capable of accurate speed control, is used to push the cone penetrometer. The cone penetration rate is set at a constant value of 2.0 mm/second in tests. The slow penetration rate is necessary to allow the reaction of lateral air pressure to reach an equilibrium in all the stress control units. However, the penetration rate is not expected to influence the test results (Dayal and Allen, 1975).

A series of cone penetration tests was performed in Da Nang sand, a clean uniformly graded quartz sand, using the simulator. The characteristics of Da Nang sand will be described later. Figure 6 shows the q_c profiles under simulated field conditions (referred to as B5), where $\sigma'_{vo}=43.7$ kPa and $\sigma'_{ho}=22$ kPa, with R_d values of 18 and 22 and D_r values of 65% and 84%. The average of the q_c values at depths from 600 to 1200 mm was taken as the representative value. Results show that q_c of two R_d values agree within 6.9% for D_r of 65% and within 0.1% for D_r of 84%. The similarity of q_c under two different R_d values indicates that the boundary effects were substantially reduced.

IV. Characteristics of Da Nang Sand

A batch of quartz sand from Da Nang, Vietnam, was used to provide specimens for laboratory experiments. According to the grain size distribution curve

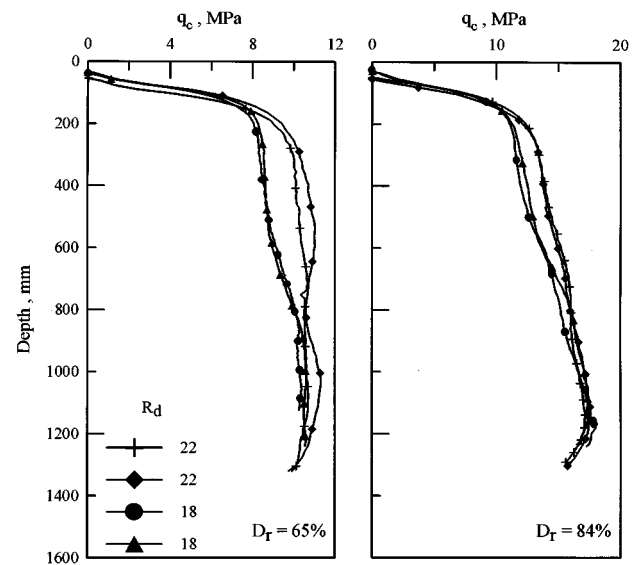


Fig. 6. q_c profiles under simulated field conditions with D_r values of 65% and 84%

shown in Fig. 7, Da Nang sand (DNS) is uniformly graded, has an average grain diameter, D_{50} , of 1.1 mm, and a coefficient of uniformity, C_u , of 1.74. The specific gravity G_s of DNS is 2.61. The maximum dry unit weight (γ_{dmax}) was 16.87 kN/m³, and the minimum dry unit weight (γ_{dmin}) was 14.13 kN/m³. According to scanning electron microscope (SEM) photographs taken of sand particles, DNS is sub-angular to angular.

A series of isotropically consolidated drained triaxial (CID) tests was performed with volume change measurements to determine the strength and dilatancy characteristics of DNS. The triaxial specimens were sheared by means of axial compression. The D_r and effective confining stress (σ'_c) applied in this series of triaxial tests are summarized in Table 3.

Bolton (1986) used a saw blade model of dilatancy to describe the shearing behavior of sand. The trace of shearing development is similar to the shape of a saw blade between the contact surfaces of particles. On the inclined surface, the friction angle (ϕ'_{crit}) can be considered as a shearing occurred under in the critical state, where shearing continues without volume change. In order to slide upwards along the saw blade, another dilatancy angle (ψ) is necessary. The friction angle (ϕ'_{crit}) on the sliding surface and the overriding capability comprise the apparent angle of shearing resistance (ϕ'). ϕ'_{crit} is a function of the mineral content of the sand and can be obtained under the critical state. The characteristics of the dilatancy of sands are affected by sand density and confining stress. Bolton

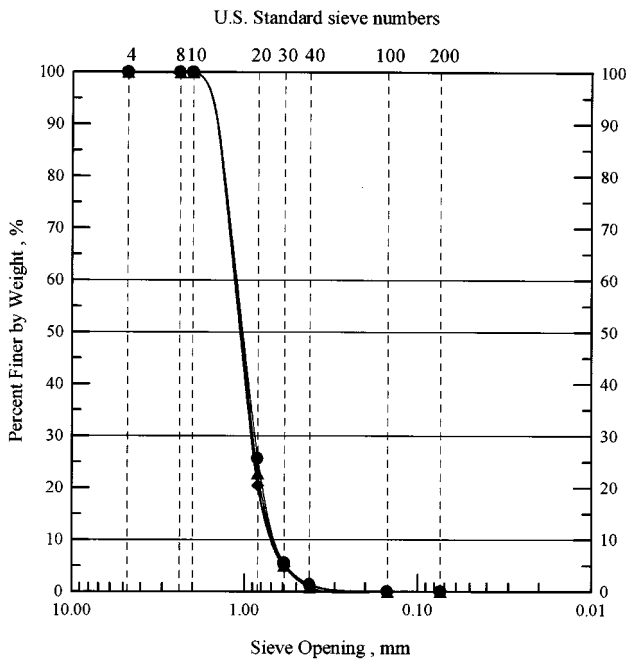


Fig. 7. Grain size distribution of Da Nang sand.

Table 3. Variables Applied in the CID Tests

D_r , %	50	65	84		
σ'_c , kPa	43.7	98.1	147.2	245.3	392.4

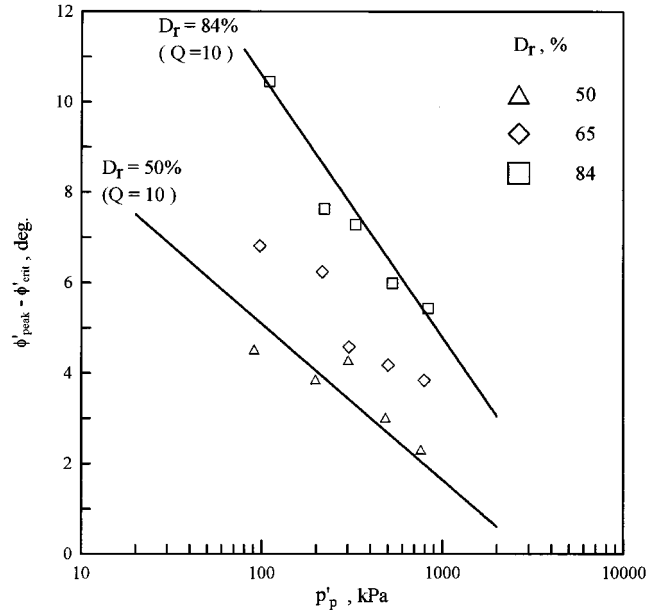


Fig. 8. $\phi'_{peak} - \phi'_{crit}$ versus p'_p .

(1986) proposed a relative dilatancy index I_R to present the global effect, which can be expressed as

$$I_R = \frac{D_r}{100}(Q - \ln p'_p) - 1, \quad (3)$$

where

Q = an empirical constant that varies with the crushing strength of the grains; for quartz and feldspar, $Q=10$;

p'_p = the mean effective stress at peak deviator stress.

The correlation between I_R and the friction angle is given by

$$\phi'_{peak} - \phi'_{crit} = 3I_R^o, \quad (4)$$

where

ϕ'_{peak} = the friction angle at peak deviator stress.

Figure 8 shows a plot of $\phi'_{peak} - \phi'_{crit}$ versus p'_p from triaxial tests on DNS, where ϕ' is obtained by dropping

Calibration of Cone Penetration Test in Sand

Table 4. Variables Applied in the CPT under B5 Conditions

D_r , %	50	65	84
K	0.5	1.0	2.0
σ'_{oo} ^a , kPa	29.2	43.7	98.1
			147.2

$$^a \sigma'_{oo} = \frac{1}{3}(\sigma'_{vo} + 2\sigma'_{ho})$$

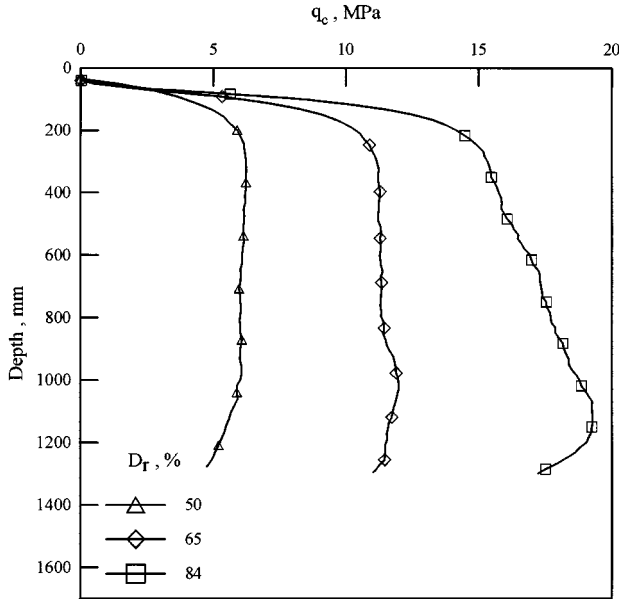


Fig. 9. q_c profiles of different D_r values under simulated field conditions.

a tangent from the origin onto a single Mohr circle of effective stress. A Q value of 10 would give a reasonable fit to the data points in Fig. 8 using Eq. (3). This would indicate that DNS is comparable to the quartz sand (e.g., Ottawa sand) reported by Bolton (1986). ϕ'_{crit} is 33.4° from triaxial tests on loose DNS specimens.

Dilatancy is believed to have a marked influence on q_c values, as indicated by the results of previous studies (Yu and Houlsby, 1991; Huang and Ma, 1994; Salgado *et al.*, 1997). The boundary effects under B1 or B3 in a conventional chamber a direct reflections of the sand dilatancy, as will be discussed later.

V. Evaluation of q_c in Sand under Simulated Field Conditions

A series of cone penetration tests under B5 conditions was conducted in the simulator. For comparison purposes, a limited number of additional CPT were conducted under B1 conditions in the same simulator.

Table 4 summarizes the variables applied in the calibration tests under B5 conditions. A standard size cone with a cross sectional area A_c of 10 cm^2 ($R_d=22$) was used for all of the tests.

The q_c profiles of different D_r from CPT under the same initial boundary conditions ($\sigma'_{oo}=43.7 \text{ kPa}$ and $K=1.0$) are shown in Fig. 9. The results show that a plateau of the q_c value is generally reached at depths of 250 and 300 mm for D_r of 50% and 65%, respectively. For $D_r=84\%$, a stabilized q_c develops at depths in excess of 300 mm. In order to analyze the test results, the average q_c values were taken at depths from 400 to 1000 mm for D_r of 50%, and from 600 to 1200 mm for D_r of 65% and 84%.

Figure 10 shows the ΔC measurements and P_{ro} applied to ring No. 10 (midheight of the specimen) during the tests depicted in Fig. 9. The depth in Fig. 10 is in reference to the cone tip level and is normalized with respect to the cone diameter D_{cone} . Figure 10 clearly demonstrates that under simulated field conditions, the lateral boundary is neither constant stress (P_{ro} is a constant) nor rigid ($\Delta C=0$). It appears that ΔC of medium dense sand ($D_r=50\%$) reaches a maximum near the cone tip and then maintains a constant value. The ΔC measurements of dense to very dense sand ($D_r=65\%$ and 84%) reach maximum values ahead of the cone tip at about 3 to 5 D_{cone} and then decrease slightly but consistently as the cone tip passes. It should be noted that at D_r of 84%, ΔC is smaller, but P_{ro} is much higher than that at D_r of 50% and 65%. For very dense sand, the rigidity causes the applied pressure P_{ro} to grow rapidly and to limit the dilatancy

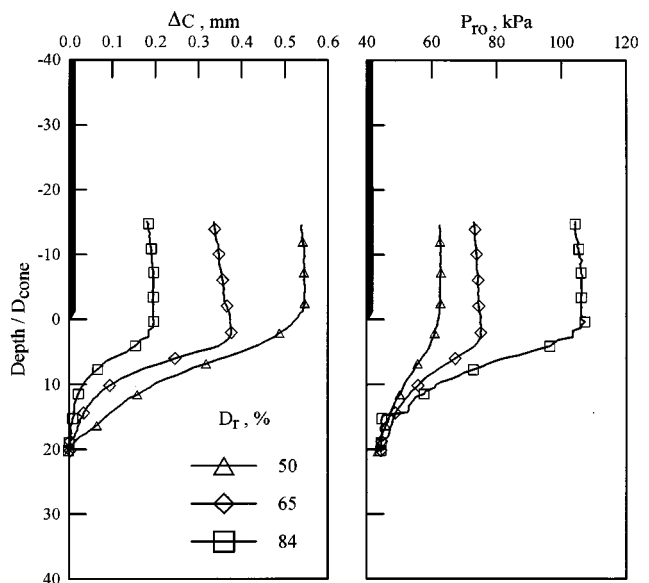


Fig. 10. ΔC and P_{ro} measurements at ring No. 10.

of the sand.

Figure 11 shows q_c versus σ'_{vo} . For a given σ'_{vo} , the corresponding q_c can vary by as much as 50% from the mean value. The test results indicate there is no unique relationship between q_c and σ'_{vo} . Similar findings have also been reported by others (Houlsby and

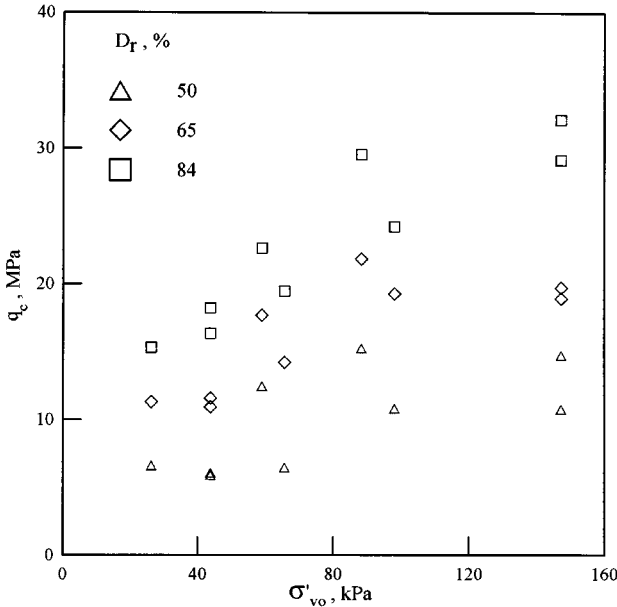


Fig. 11. Measured q_c versus σ'_{vo} .

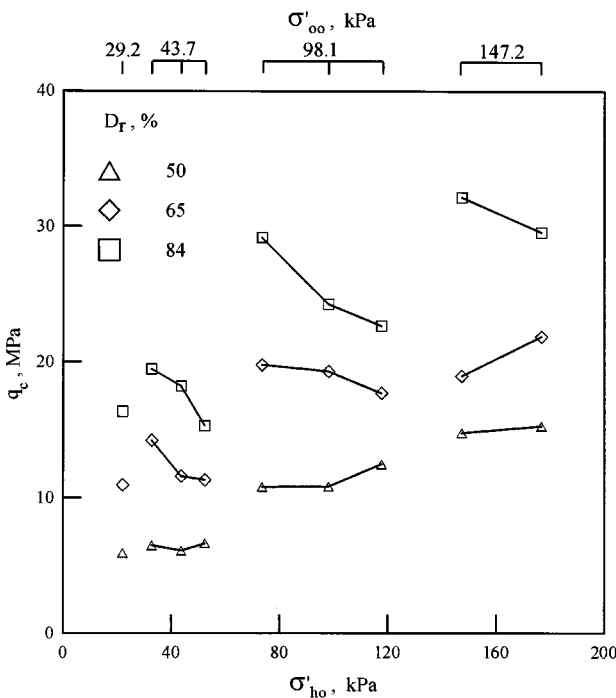


Fig. 12. Measured q_c versus σ'_{ho} .

Table 5. Comparison of Tests under B1 and B5 Conditions

Test No.	Boundary condition	D_r , %	σ'_{ho}	σ'_{vo}	σ'_{hc}	q_c
				kPa		MPa
B5-1	B5	50	43.7	43.7	53.5	6.1
B5-2	B5	65	43.7	43.7	73.1	11.6
B5-3	B5	84	43.7	43.7	98.5	18.2
B1-1	B1	50	53.5	43.7	-	5.7
B1-2	B1	65	73.1	43.7	-	10.9
B1-3	B1	84	98.5	43.7	-	18.5

Hitchman, 1988).

As shown in Fig. 12, the correlation between q_c and σ'_{ho} appears to be scattered. This is different from previous studies that related q_c to σ'_{ho} (Baldi *et al.*, 1986; Houlsby and Hitchman, 1988; Jamiolkowski *et al.*, 1988). This scattering, however, is not random. When the scale is large, there is a positive relationship between q_c and σ'_{ho} . When D_r is larger than 50%, there exists a localized (i.e., under the same D_r and σ'_{oo}) negative relationship between q_c and σ'_{ho} . Apparently, the higher value of σ'_{ho} prohibits dilatancy; hence, there is less lateral expansion on the physical boundary during cone penetration.

In most cases, the horizontal stress at the physical boundary (P_{ro} in Fig. 10) remains more or less a constant after reaching a peak value. This peak P_{ro} is chosen to represent a stabilized horizontal stress measured at the physical boundary after cone tip passage and will be referred to as σ'_{hc} . For all the available tests under B5 conditions, a clear and positive relationship between q_c and σ'_{hc} was obtained as shown in Fig. 13. This result parallels the findings reported by Houlsby and Hitchman (1988), where comparisons were made between q_c and σ'_{ho} under B1 conditions.

For comparison purposes, a set of calibration tests under B5 conditions (i.e., tests B5-1, B5-2, and B5-3 in Table 5) were duplicated under B1 conditions (i.e., tests B1-1, B1-2 and B1-3 in Table 5). The respective σ'_{hc} values recorded in tests B5-1, B5-2, and B5-3 were applied as the corresponding horizontal stress values in tests B1-1, B1-2 and B1-3. The results show that if σ'_{hc} or the terminal horizontal stress expected at the physical boundary is applied, even B1 can properly simulate the field conditions. The q_c values obtained under B1 and B5 conditions agreed within 7% in these tests.

Two empirical equations, which relate q_c to the initial stress state (i.e., σ'_{oo} and σ'_{ho}), proposed respectively by Jamiolkowski *et al.* (1988) and Baldi *et al.* (1986), are chosen for comparison with the CPT results under B5 conditions (referred to as $q_{c,B5}$). Both equa-

Calibration of Cone Penetration Test in Sand

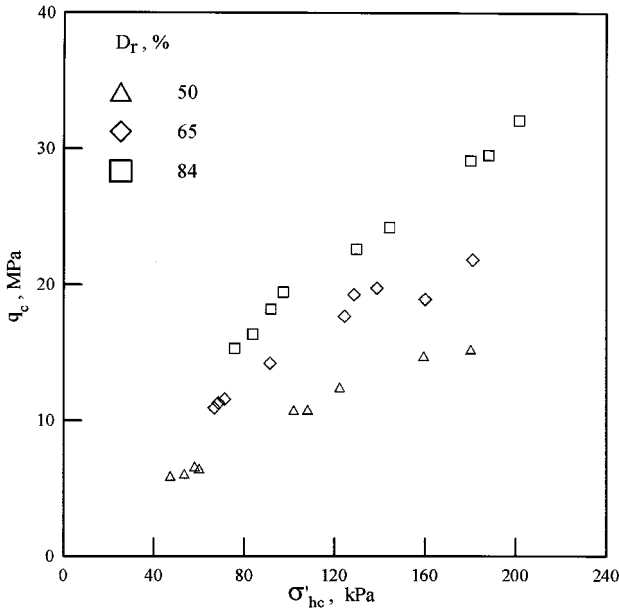


Fig. 13. Measured q_c versus σ'_{hc} .

tions were developed based on tests in Ticino sand, and the boundary effects were corrected. According to Baldi *et al.* (1986) the cone tip resistance, $q_{c,B}$ is related to the initial state of stress and D_r as follows:

$$q_{c,B} = 220p_a \left(\frac{\sigma'_{vo}}{p_a}\right)^{0.065} \left(\frac{\sigma'_{ho}}{p_a}\right)^{0.44} \exp(2.93D_r), \quad (5)$$

where

p_a = the reference pressure (1 kPa).

Jamiolkowski *et al.* (1988) related the cone tip resistance, $q_{c,J}$, to σ'_{oo} as follows:

$$q_{c,J} = 205p_a \left(\frac{\sigma'_{oo}}{p_a}\right)^{0.51} \exp(2.93D_r). \quad (6)$$

Comparisons of $q_{c,J}$ with $q_{c,B5}$ and of $q_{c,B}$ with $q_{c,B5}$ are, respectively, shown in Fig. 14 and Fig. 15. The $q_{c,J}/q_{c,B5}$ and $q_{c,B}/q_{c,B5}$ values range from 70 to 100%. $q_{c,J}/q_{c,B5}$ is not a constant under the same σ'_{oo} , even though $q_{c,J}$ depends upon σ'_{oo} according to Eq. (6). When $\sigma'_{oo}=43.7$ or 98.1 kPa, $q_{c,J}/q_{c,B5}$ increases with K (or σ'_{ho}) for D_r of 65 and 84%. Similar trends are also found in the comparisons between $q_{c,B5}$ and $q_{c,B}$ (Fig. 15).

According to the available CPT data under B5 conditions, a relatively consistent relationship is possible only between q_c and σ'_{oo} as shown in Fig. 16. Based on the statistical optimization method, the empirical equation is similar to the pattern proposed by Jamiolkowski *et al.* (1988):

$$q_c = 492p_a \left(\frac{\sigma'_{oo}}{p_a}\right)^{0.46} \exp(2.23D_r). \quad (7)$$

Equation (7), depicted in Fig. 16 as solid curves, has a coefficient of correlation of 0.97 with the available test data. For comparison purposes, Eq. (6) is also

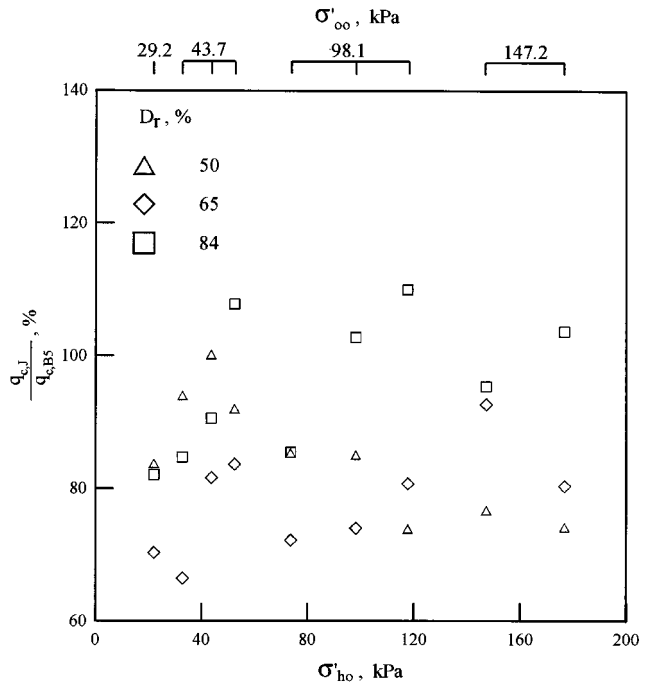


Fig. 14. Comparison of $q_{c,B5}$ and $q_{c,J}$.

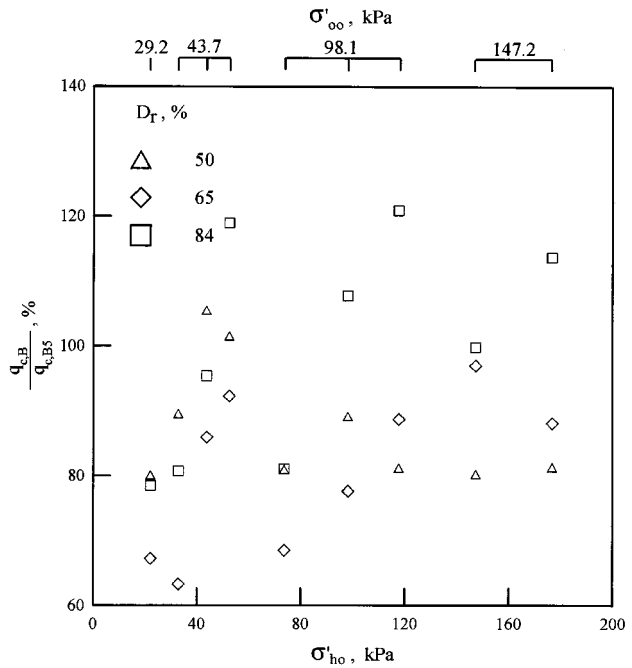


Fig. 15. Comparison of $q_{c,B5}$ and $q_{c,B}$.

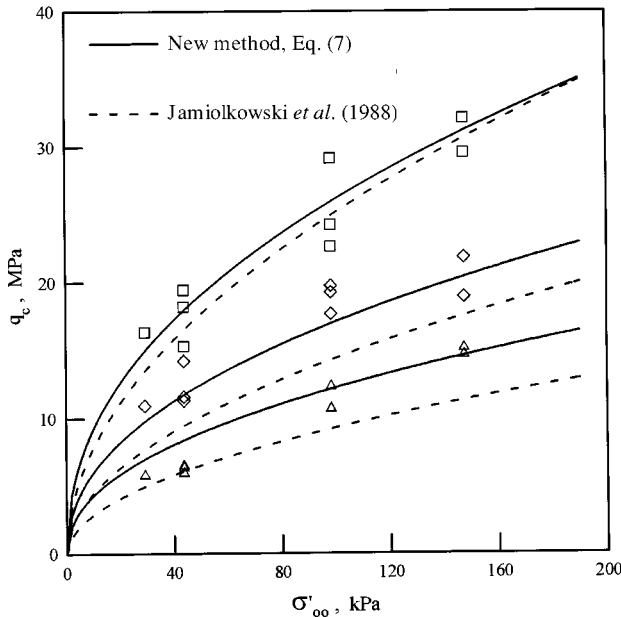


Fig. 16. Measured q_c versus σ'_{oo} .

plotted in Fig. 16 using dashed lines.

VI. Concluding Remarks

A CPT calibration system that is capable of simulating field conditions has been developed. The boundary effects can be substantially reduced using this new system. For the first time, q_c values obtained from CPT calibration tests in the new simulator can be used without the need to account for the boundary effects. Based on a series of CPT performed in the new simulator, the following conclusions can be drawn:

The relationship between q_c and the initial horizontal stress σ'_{ho} is not nearly as strong as has been reported by others. Under certain circumstances, there may even be a negative relationship between q_c and σ'_{ho} . The initial mean normal stress, σ'_{oo} , appears to have the most consistent relationship with q_c . An empirical equation developed based on CPT performed in the new simulator has a coefficient of correlation of 0.97 with the test data.

The strong correlation between q_c and the horizontal stress, observed earlier in conventional chamber tests under B1 conditions, is most likely a result of boundary effects. The lateral boundary stress is forced to be constant during cone penetration under B1 conditions. Under simulated conditions, the boundary stress varies as cone penetration continues. Test results indicate that q_c has a strong relationship with the maximum lateral stress measured at the physical specimen boundary σ'_{hc} during cone penetration. If B1 is

to be used in a conventional chamber for CPT calibration tests, it is apparent that σ'_{hc} , not σ'_{ho} , should be imposed on the lateral boundary of the chamber specimen.

Acknowledgment

This research was funded by the Sinotech Foundation for Research and Development of Engineering Sciences and Technologies, and the National Science Council of the R.O.C. under contract NSC 87-2211-E-009-034. Their support was greatly appreciated.

Nomenclature

A_c	cross sectional area of cone
C_u	coefficient of uniformity
D_r	relative density
D_{50}	average grain diameter
D	diameter of the sand specimen
D_{cone}	cone diameter
e	void ratio
F_R	sleeve friction ratio
f_s	sleeve friction resistance
G_s	specific gravity
I_R	relative dilatancy index
K	ratio of horizontal stress over vertical stress
K_O	at rest lateral earth pressure coefficient
NC	normally consolidated
OC	over consolidated
OCR	over consolidation ratio
p_a	reference pressure (1kPa)
P_1	limit pressure
P_{ro}	lateral stress at the physical-simulated soil mass interface
p'_p	mean effective stress under peak deviator stress conditions
Q	empirical constant that varies with the crushing strength of sand grains
q_c	cone tip resistance
$q_{c,B}$	q_c obtained from the empirical equation proposed by Baldi <i>et al.</i> (1986)
$q_{c,B5}$	q_c obtained under simulated field conditions (B5)
$q_{c,J}$	q_c obtained from the empirical equation proposed by Jamiolkowski <i>et al.</i> (1988)
R_d	diameter ratio of the physical sand specimen over that of the cone
r	chamber size correction factor
γ_{dmax}	maximum dry density
γ_{dmin}	minimum dry density
ΔC	circumferential displacement at physical boundary of the ring chamber
ϵ_r	radial normal strain
ϵ_{ro}	radial normal strain at the physical-simulated soil mass interface
σ_{ho}	initial or field horizontal stress
σ'_c	effective confining stress applied in the triaxial tests
σ'_{hc}	peak p_{ro} under simulated field conditions
σ'_{ho}	initial (prior to cone penetration) horizontal effective stress
σ'_{oo}	mean effective normal stress = $\frac{1}{3}(\sigma'_{vo} + 2\sigma'_{ho})$
σ'_{vo}	vertical effective stress
ϕ'	drained friction angle
ϕ'_{crit}	drained friction angle under critical state, where shearing continues without volume change

Calibration of Cone Penetration Test in Sand

ϕ'_{peak}	drained peak friction angle
$\phi(\epsilon_r)$	radial strain and stress relationship of the sand specimen
ψ	dilatancy angle

References

- Baldi, G., R. Bellotti, V. Ghionna, M. Jamiokowski, and E. Pasqualini (1982) Design parameters for sands from CPT. *Proceedings of the Second European Symposium on Penetration Testing*, Amsterdam, Holland.
- Baldi, G., R. Bellotti, V. Ghionna, M. Jamiokowski, and E. Pasqualini, (1986) Interpretation of CPTs and CPTUs—part II: drained penetration in sands. *Proceedings of the Fourth International Geotechnical Seminar on Field Instrumentation and in Situ Measurements*, Nanyang Technological Institute, Singapore.
- Baligh, M. M. (1976) Cavity expansion in sands with curved envelopes. *Journal of Geotechnical Engineering Division, ASCE*, **102**(11), 1131-1146.
- Been, K. and K. M. Kosar (1991) Hydraulic fracture simulations in a calibration chamber. *Proceedings of the First International Symposium on Calibration Chamber Testing*, Potsdam, NY, U.S.A.
- Been, K., J. H. A. Crooks, and L. Rothenburg, (1988) A critical appraisal of CPT calibration chamber tests. *Proceedings of the First International Symposium on Penetration Testing (ISOPT-1)*, Orlando, FL, U.S.A.
- Bolton, M. D. (1986) The strength and dilatancy of sands. *Geotechnique*, **36**(1), 65-78.
- Borden, R. H. (1991) Boundary displacement induced by DMT penetration. *Proceedings of the First International Symposium on Calibration Chamber Tests*, Potsdam, NY, U.S.A.
- Chapman, G. A. and I. B. Donald (1981) Interpretation of static penetration tests in sand. *Proceedings of the 10th International Conference on Soil Mechanics and Foundation Engineering*, Stockholm, Sweden.
- Dayal, U. and J. H. Allen (1975) The effect of penetration rate on the strength of remolded clay and sand samples. *Canadian Geotechnical Journal*, **3**, 336-348.
- Durgunoglu, H. T. and J. K. Mitchell (1975) Static penetration resistance of soils. I. Analysis. II. Evaluation of theory and implications for practice. *Proceedings of Specialty Conference on In-Situ Measurement of Soil Properties*, ASCE, Raleigh, NC, U.S.A.
- Ghionna, V. N. and M. Jamiolkowski (1991) A critical appraisal of calibration chamber testing of sands. *Proceedings of the First International Symposium on Calibration Chamber Testing*, Potsdam, NY, U.S.A.
- Holden, J. C. (1991) History of the first six CRB calibration chambers. *Proceedings of the First International Symposium on Calibration Chamber Testing*, Potsdam, NY, U.S.A.
- Houlsby, G. T. and R. Hitchman (1988) Calibration chamber tests of a cone penetrometer in sand. *Geotechnique*, **38**(1), 39-44.
- Hsu, H. H. and A. B. Huang (1998) Development of an axisymmetric field simulator for cone penetration tests in sand. *ASTM Geotechnical Testing Journal*, **21**(4), 348-355.
- Huang, A. B., R. D. Holtz, and J. L. Chameau (1991) A laboratory study of pressuremeter tests in clays. *Journal of Geotechnical Engineering Division, ASCE*, **117**, 1549-1567.
- Huang, A. B. and M. Y. Ma (1994) An analytical study of cone penetration tests in granular material. *Canadian Geotechnical Journal*, **31**(1), 91-103.
- Jamiolkowski, M., V. N. Ghionna, R. Lancellotta, and E. Pasqualini (1988) New correlations of penetration tests for design practice. *Proceedings of the First International Symposium on Penetration Testing (ISOPT-1)*, Orlando, FL, U.S.A.
- Janbu, N. and K. Senneset (1974) Effective stress interpretation of in situ static penetration tests. *Proceedings of the European Symposium on Penetration Testing*, Stockholm, Sweden.
- Kulhawy, F. H. (1991) Fifteen+ years of model foundation testing in large chambers. *Proceedings of the First International Symposium on Calibration Chamber Tests*, Potsdam, NY, U. S.A.
- Mayne, P. W. and F. H. Kulhawy (1991) Calibration chamber database and boundary effects correction for CPT data. *Proceedings of the First International Symposium on Calibration Chamber Testing*, Potsdam, NY, U.S.A.
- O'Neill, M. W. (1991) Houston's calibration chamber: case history. *Proceedings of the First International Symposium on Calibration Chamber Tests*, Potsdam, NY, U.S.A.
- Parkin, A. K. (1988) The calibration of cone penetrometers. *Proceedings of the First International Symposium on Penetration Testing (ISOPT-1)*, Orlando, FL, U.S.A.
- Parkin, A. K. and T. Lunne (1982) Boundary effects in the laboratory calibration of a cone penetrometer for sand. *Proceedings of the Second European Symposium on Penetration Testing*, Amsterdam, Holland.
- Peterson, R. W. and K. Arulmoli (1991) Overview of a large stress chamber system. *Proceedings of the First International Symposium on Calibration Chamber Tests*, Potsdam, NY, U.S.A.
- Rad, N. S. and M. T. Tumay (1987) Factors affecting sand specimen preparation by raining. *ASTM Geotechnical Testing Journal*, **10**(1), 31-37.
- Robertson, P. K., R. G. Campanella, D. Gillespie, and J. Grieg (1986) Use of piezometer cone data. *Proceedings of In-Situ '86, ASCE, Specialty Conference*, Blacksburg, VA, U.S.A.
- Salgado, R. (1993) *Analysis of Penetration Resistance in Sands*. Ph.D. Dissertation. Department of Civil Engineering, University of California at Berkeley, Berkeley, CA, U.S.A.
- Salgado, R., J. K. Mitchell, and M. Jamiolkowski (1997) Cavity expansion and penetration resistance in sand. *Journal of Geotechnical and Geoenvironmental Engineering, ASCE*, **123**(4), 344-354.
- Schmertmann, J. H. (1976) *An Updated Correlation between Relative Density D_r and Fugro-Type Electric Cone Bearing q_c* . DACW 39-76 M6646, Waterways Experiment Station, U.S.A.
- Veismanis, A. (1974) Laboratory investigation of electrical friction cone penetrometers in sands. *Proceedings of European Symposium on Penetration Testing*, Stockholm, Sweden.
- Vesic, A. S. (1972) Expansion of cavities in infinite soil mass. *Journal of Soil Mechanics and Foundations Division, ASCE*, **98**, 265-290.
- Villet, W. C. B. and J. K. Mitchell (1981) Cone resistance, relative density and friction angle. *Proceedings of ASCE Symposium on Cone Penetration Testing and Experience*, St. Louis, MO, U.S. A.
- Yu, H. S. and G. T. Houlsby (1991) Finite cavity expansion in dilatant soils: loading analysis. *Geotechnique*, **41**(2), 173-183.

圓錐貫入試驗在砂土中之標定

許懷後 黃安斌

國立交通大學土木工程學系

摘 要

圓錐貫入試驗由於操作簡單，是一種常用的現地試驗方法。對於不易取得非擾動土樣的砂土層而言，圓錐貫入試驗是極佳的現地量測方式。由於圓錐貫入土壤中是一種大應變的行為，要以理論分析的方法來合理的解釋試驗結果，有其限制性與困難度。所以對於所擷取資料的分析與解釋，則大多由經驗公式而來。而經驗公式大多來自於試驗室中的標度試驗。標度試驗的重要缺陷是它的邊界效應。有人提出以修正係數的方法來抵消邊界效應，但是修正係數方法的正確性與邊界影響之機制至今都尚未得到證實。作者已研發完成一套能夠降低邊界效應以達到模擬現地情況的標度槽系統。為推求錐尖阻抗與應力狀態間的關係，已經在此新研發的標度槽系統中完成一系列的圓錐貫入標度試驗。試驗結果顯示，錐尖阻抗與初始平均有效應力間較具有關連性。雖然與初始橫向應力間並無一明確的關係，但是在平均有效應力相同的前提下，可以有一致性的關係。此外，錐尖阻抗受錐尖附近之橫向應力影響，彼此間可發現一明確的關係。本文介紹圓錐貫入標度試驗、敘述此新研發之標度槽、並探討在模擬現地情況下，錐尖阻抗與應力狀態間的關係。